Eva1 maintains the stem-like character of glioblastoma-initiating cells by activating the non-canonical NF-κB signaling pathway

Naoki Ohtsu[1], Yuka Nakatani[2,4], Daisuke Yamashita[3], Shiro Ohue[3], Takanori Ohnishi[3], and Toru Kondo[1,2]

[1]Division of Stem Cell Biology, Institute for Genetic Medicine, Hokkaido University, Sapporo, Hokkaido 060-0815, Japan, [2]Laboratory for Cell Lineage Modulation, RIKEN Center for Developmental Biology, Kobe 650-0047, Japan, [3]Department of Neurosurgery, Ehime University Graduate School of Medicine, To-on, Ehime 791-0295, Japan. [4]Present address: Division of Bio-Function Dynamics Imaging, Center for Life Science Technology, RIKEN, Kobe, Hyogo 650-0047, Japan

Correspondence: tkondo@igm.hokudai.ac.jp

Running head: Eva1 is a novel GIC regulator

Keywords: Glioblastoma (GBM)/GBM-initiating cells (GICs)/Eva1/non-canonical NF-κB

Conflicts of Interest: No potential conflicts of interest were disclosed

Abstract

Glioblastoma (GBM)-initiating cells (GICs) are a tumorigenic subpopulation that are resistant to radio- and chemotherapies and are the source of disease recurrence. Therefore, the identification and characterization of GIC-specific factors is critical towards the generation of effective GBM therapeutics. In this study, we investigated the role of Epithelial V-like antigen 1 (Eva1, also known as myelin-like protein Zero like-2) in stemness and GBM tumorigenesis. Eva1 was prominently expressed in GICs in vitro and in stem cell marker (Sox2, CD15, CD49f)-expressing cells derived from human GBM tissues. Eva1 knockdown in GICs reduced their self-renewal and tumor-forming capabilities, whereas Eva1 overexpression enhanced these properties. Eva1-deficiency was also associated with decreased expression of stemness-related genes, indicating a requirement for Eva1 in maintaining GIC pluripotency. We further demonstrate that Eva1 induced GIC proliferation through the activation of the RelB-dependent non-canonical NF-κB pathway by recruiting TRAF2 to the cytoplasmic tail. Taken together, our findings highlight Eva1 as a novel regulator of GIC function and also provide new mechanistic insight into the role of non-canonical NF-κB activation in GIC, thus offering multiple potential therapeutic targets for preclinical investigation in GBM.

Introduction

Gliomas are brain tumors possessing the characteristics of glial cells, astrocytes, and oligodendrocytes, and have been classified into four grades (WHO grade I-IV) based on their pathological features. Glioblastoma (GBM) is the most malignant glioma (WHO grade IV), and patients with GBM have a median survival of approximately one year. In spite of tremendous efforts to effectively treat GBM, the overall survival rates of patients with GBM have remained unchanged over the past few decades.

The discovery of GBM-initiating cells (GICs) has had a significant impact on GBM research (1). GICs have a strong self-renewal capability, express stem cell markers, such as CD133 (also known as Prominin1), Sox2, CD15 (also known as Stage-Specific Embryonic Antigen 1 and Lewis X), and CD49f (also known as integrin α 6), and are more resistant to radio- and chemo-therapies higher than non-GICs (2-5). GICs have also been shown to exploit the signaling pathways that are involved in the maintenance of neural stem cells (NSCs) (2-5). NSCs exist only in the subventricular zone and hippocampus (6,7), both of which contain a special microenvironment (niche) for the maintenance of NSCs, whereas GBM arises in many areas in the brain. It currently remains unknown how GICs maintain their stemness in the brain; whether GICs generate their preferable niche anywhere or employ an unknown mechanism for their maintenance in non-NSC niches.

We previously established the mouse GIC lines (mGICs), NSCL61 and OPCL61, by overexpressing an oncogenic $HRas^{L61}$ in *p53*-deficient NSCs and oligodendrocyte precursor cells (OPCs), respectively (8,9). These mGICs formed transplantable GBM with hypercellularity, pleomorphism, multinuclear giant cells, mitosis, and necrosis, even when as few as ten cells were injected into the brains of nude mice. These findings indicated that they were highly enriched in bona fide GICs.

Using DNA microarray analysis, we compared the gene expression profiles of mGICs with those of their parental cells and identified genes that increased and decreased in mGICs. By evaluating the candidate genes using human GICs (hGICs) and GBM tissues, we have successfully selected potential GIC-specific genes (8-11).

Among the candidate genes evaluated, we focused on Epithelial V-like antigen 1 (Eva1, also known as myelin protein Zero-like 2). Eva1 was originally identified as an immunoglobulin superfamily member expressed on the developing thymus epithelial cell membrane and disappeared in the developed one (12-14). Eva1 was also shown to be involved in the T cell development through the Eva1-Eva1 homophilic interaction between CD4/CD8 double-positive cells and thymus epithelial cells in the early embryo (12-14), however there was no detectable phenotype, including the hematopoietic development, in the Eva1 knockout mice (12-15, Ohtsu et al, unpublished observation). Notably, it has not been shown that Eva1 was involved in either tumorigenesis or stemness. These findings led us to investigate whether Eva1 can be a novel GIC marker and/or a potential therapeutic target.

Here we show the evidence that Eva1 is expressed on GICs and its modulation impacts GIC characteristics, including stemness-related gene expression, side population, self-renewal activity and tumorigenesis, through the non-canonical NF-κB signaling pathway, providing a new molecular mechanism that maintains GIC characteristics.

Materials and Methods

Animals and Chemicals

Mice were obtained from the Laboratory for Animal Resources and Genetic Engineering at the RIKEN Center for Developmental Biology (CDB) and from Charles River Japan, Inc. All mouse experimental protocols were approved by the Animal Care and Use Committees of RIKEN CDB, Ehime University, and Hokkaido University. Chemicals and growth factors were purchased from Sigma-Aldrich and Peprotech, respectively, except where otherwise indicated.

Cell culture

Mouse primary NSCs, NSCL61 cells, human NSCs (hNSCs, Invitrogen) and GICs (hGICs, E2, E3 and E6) were cultured in DMEM/F12 (Gibco, BRL) supplemented with bFGF (10 ng/ml) and EGF (10 ng/ml) (NSC medium), as described previously (8-11,16). For immunostaining, cells were cultured in chamber slides (Nunc) precoated with fibronectin and poly-D-lysine, as described previously (16).

Immunochemistry

Immunostaining of paraffin-embedded human brain-tumor sections (6 μm thick) and mouse cells or brain sections was performed as described previously (8). Eva1 was retrieved by HistoVT One according to the supplier's instructions (Nacalai Tesque). The sections were permeabilized with 0.3% TritonX-100 in PBS for penetration, treated with a blocking solution (2% skim milk, 0.3% Triton X-100, and PBS) for 1 h, and incubated with primary antibodies for 16 h at 4°C. Cells were fixed and immunostained as described previously (16). The following antibodies were used to detect antigens: rabbit polyclonal anti-Eva1 (10 μg/ml) produced by immunizing a

rabbit with a synthetic peptide (CPMSGRFKDRVSWDGNPE) using a standard method (Fig. S2*A* and *B*), mouse monoclonal anti-Nestin (BD; 1:200), mouse monoclonal anti-CD15 (BD Pharmingen; 1:200), mouse monoclonal anti-GFAP (Sigma; 1:400), mouse monoclonal anti-Tuj1 (Sigma, 1:400), mouse monoclonal anti-O4 (hybridoma supernatant, 1:4), biotinylated mouse monoclonal anti-CD49f (Affymetrix; 1:100), biotinylated goat polyclonal anti-human Sox2 (R&D; 1:200) and mouse monoclonal anti-RORγT (Millipore, 1:100). Antibodies were detected with Alexa568-conjugated goat anti-mouse IgG (Molecular Probe; 1:500), Alexa488-conjugated goat anti-rabbit (Molecular Probe; 1:500), and streptoavidine-Cy3 (Jackson ImmunoResearch; 1:500). Cells were counterstained with DAPI (1 μg/ml) to visualize the nuclei. Fluorescence images were obtained using an AxioImager A1 microscope (Carl Zeiss).

Flow cytometry

Flow cytometry was performed as described previously (11). The following antibodies were used to detect antigens: rabbit polyclonal anti-Eva1 (5 μ g/ml), mouse monoclonal anti-CD15 (5 μ g/ml; BD Pharmingen) and biotinylated mouse monoclonal anti-CD49f (Affymetrix; 1:100). Antibodies were detected with APC-conjugated goat anti-mouse IgG (Santa Cruz Biotech.; 1:200) and PE-conjugated goat anti-rabbit IgG (Santa Cruz Biotech.; 1:200). The cells were analyzed in an Aria II (Becton Dickinson) using a dual-wavelength analysis (488 nm solid-state laser and 638 nm semiconductor laser). Propidium iodide (PI)-positive (i.e., dead) cells were excluded from the analysis.

The SP was analyzed as shown previously (15). Reserpine (10 μ M), an inhibitor of some ABC transporters, was used to identify SP.

Human brain tumors

Human GICs were used according to the research guidelines of the Ehime University Graduate School of Medical Science and the Hokkaido University Institute for Genetic Medicine. Poly(A)+ RNA was prepared using a QuickPrep mRNA Purification Kit (GE Healthcare). Control human brain total mRNA (CB) was purchased from Invitrogen. cDNA was synthesized using a Transcription First Strand cDNA Synthesis Kit (Roche).

Intracranial cell transplants in the NOD/SCID mouse brain and brain-tumor histopathology

NSCL61 cells or hGICs were suspended in 5 μl of culture medium and injected into the brains of 5- to 8-week-old female NOD/SCID mice under anesthesia with 10% pentobarbital. The stereotactic injection coordinates were 2 mm forward from the lambda, 2 mm lateral from the sagittal suture, and 5 mm deep.

Mouse brains were dissected, fixed in 4% paraformaldehyde at 4°C overnight, transferred to 70% ethanol, processed on Tissue-Tek VIP (Sakura Finetek Japan, Tokyo, Japan), and embedded in paraffin. Coronal sections (6-μm thick) from the cerebral cortex were prepared on a microtome and stained with hematoxylin-eosin (HE).

RT-PCR

RT-PCR was performed as described previously (16), with the cycle parameters of 20 sec at 94°C, 30 sec at 57°C, and 60 sec at 72°C for 35 cycles (GICs) or 40 cycles (GBM tissues). Cycles for *gapdh* were 15 sec at 94°C, 30 sec at 53°C, and 90 sec at

72°C for 22 cycles. The following oligonucleotide DNA primers were synthesized: for *eva1*, as follows: 5' primer, 5'- TTCTCCAGCTTTGCCCCTGT-3'; 3' primer, 5'-CCGCCCATCGCTTTTTCCGG-3'. The primers for *gapdh* were as described previously (14).

Vector construction

Complementary DNAs (cDNAs) were cloned as described previously (8). Human *eva1* cDNA was inserted into the pMX-EGFP, pcDNA3.1-hyg (Invitrogen), and pcDNA3-2xFLAG-c vectors to produce pMX-EGFP-hEva1, pcDNA3.1-hyg-hEva1, and pcDNA3-hEva1-2xFLAG-c, respectively. The following oligonucleotide DNA primers were synthesized to amplify full human *eva1* cDNA: 5' primer, 5'-CGCCACCATGTATGGCAAGAGCTCTACTC-3'; 3' primer, 5'-CTTAGTCTGTGTCTTCTAAATAAACA-3'. To construct the FLAG-tagged human *eva1* expression vector, the following oligonucleotide DNA primers were synthesized: 5' primer, 5'-TGAATTCGCCACCATGTATGGCAAGAGCTCTACTC-3'; 3' primer, 5'-ACTCGAGGTCTGTGTCTTCTAAATAAACA-3'.

To knockdown mouse and human *eva1* and mouse *relb*, short-hairpin (sh) sequences were generated using InvivoGen's siRNA Wizard (http://www.sirnawizard.com/). We used the mouse *rela* sh sequence described previously (17). These sh sequences were inserted into a psiRNA-h7SKhygro G1 expression vector (InvivoGen) to produce psiRNA-h7SKhygro-meva1sh, psiRNA-h7SKhygro-heva1sh1, psiRNA-h7SKhygro-heva1sh2, psiRNA-h7SK-relash (relash), and psiRNA-h7SK-relbsh (relbsh). The knockdown efficiency of these vectors was analyzed by Western blotting (Figure S3 and S7*A*). The sh target sequences for mouse *eva1* was 5'-GCAGTCAACGGGACAGATGTT-3'; for human *eva1* were 5'-

GTGCACACTGTACGCTTCTCT-3' (sh1) and 5'-GGTGATGCTCTAACAGTGACC-3' (sh2); for mouse *rela* and *relb* were 5'-GAAGAAGAGTCCTTTCAAT-3' and 5'-ACGAGTACATCAAGGAGAAC-3', respectively. The control sh target (*egfp*) sequence was 5'-GCAAGCTGACCCTGAAGTTCA-3'.

Vectors to monitor AP1, SP1, and NF-κB were constructed by inserting oligonucleotides containing four responsible elements (RE) of the transcription factors into the pGL3 promoter vector (Promega) to produce pGL3-AP1RE, pGL3-SP1RE, and pGL3-NF-κBRE. The sequences for AP1-RE, SP1-RE, and NF-κB-RE were 5'-TGACTAATGACTAATGACTAATGACTAATGACTAATGACTAA-3', 5'-AGGGGGCGGGGTAGGGGGCGGGGTAGGGGGCGGGGTAGGGGGCGGGGT-3', and 5'-GGGAATTTCCGGGGCTTTCCGGGAATTTCCGGGGACTTTCCGGGAATTTCC-3', respectively.

The nucleotide sequences of cloned cDNA were verified using the BigDye Terminator Kit version 3.1 (Applied Biosystems) and ABI sequencer model 3130xl (Applied Biosystems).

We transfected the cells with the vectors using either the Nucleofector device according to the supplier's instructions (Lonza) or Polyethylenimine (PEI), as previously described (7,18).

Cytotoxicity assay

To examine the function of the NF-κB signaling pathway in GICs, mouse and human GICs were cultured in various concentrations of CAPE (Calbiochem), pterostilbene

(Tokyo Chemical Industry Co., LTD.) or DMSO alone (control) for 3 days and assayed for viability by the MTT assay as described previously (8).

Gene microarray and pathway analyses

A 3D-Gene Mouse Oligo chip 24k (23,522 distinct genes, Toray) was used in the DNA microarray analysis. Total RNA was labeled with Cy5 using the Amino Allyl Message AMP II aRNA Amplification Kit (Applied Biosystems). The Cy5-labeled aRNA pools were hybridized to the microarray according to the supplier's protocols (www.3d-gene.com). Hybridization signals were scanned using the ScanArray Express Scanner (Perkin Elmer) and were processed by GenePixPro version 5.0 (Molecular Devices). The raw data of each spot was normalized by substitution with the mean intensity of the background signal, as determined by all blank spot signal intensities with 95% confidence intervals. Raw data intensities greater than 2 standard deviations (SD) of the background signal intensity were considered to be valid. The signals detected for each gene were normalized by the global normalization method (the median of the detected signal intensity was adjusted to 25). Transcription factor network analysis was performed using the Network analysis software in MetaCore^{TM} (GeneGO).

Accession number for microarray data: http://www.ncbi.nlm.nih.gov/geo/query/acc.cgi?acc=GSE72849.

Immunoprecipitation and Western blotting

Immunoprecipitation was performed as previously described (19). Cell lysates were incubated with Protein G sepharose (GE Healthcare) and the anti-Eva1 (2 μg/ml)

antibody for 4 h at 4°C. The mixtures were centrifuged, and the precipitants were triple-washed and analyzed by Western blotting.

Western blotting was performed as previously described (19). The blotted membranes were probed with an anti-Eva1 (2 μg/ml), rabbit anti-NF-κB2 (Cell Signaling Technology, 1:500), mouse anti-cIAP (R&D Systems, 1:500), rabbit anti-TRAF2 (Cell Signaling Technology, 1:500), rabbit anti-NIK (Cell Signaling Technology, 1:500), anti-RelA (SIGMA, 1:500), anti-RalB (Cell Signaling Technology, 1:500), or mouse anti-GAPDH antibody (Chemicon, 1:1000). An ECL system (Amersham) was used for detection.

Luciferase assay

Luciferase was assayed as described previously (19). Using PEI, NSCL61 cells were transfected with either the *heva1* expression vector or *relash* or *relbsh* shRNA expression vector. The cells were cultured in the presence of Hygromycin B (0.2 mg/ml). NSCL61 cells were also infected with a recombinant retrovirus encoding T2DN, and DsRed+ cells were purified by flow cytometry. The selected cells were then transfected with 0.3 μg of the AP1, SP1, or NF-κB reporter vectors encoding firefly luciferase, along with 0.03 μg of the internal control vector pRL-EF1 (Promega), which encoded sea pansy luciferase. After two days, the activities of the two types of luciferases were measured using the Dual-Luciferase Reporter Assay System according to the supplier's instructions (Promega).

TCGA analysis

Relationship between *eva1* expression and the prognosis of GBM patients, % survival and % disease free, was analyzed by using the cBioPortal (20,21). Each 27 microarray

data of human GBM and Lower Grade Glioma (LGG) were obtained from The Cancer Genome Atlas (TCGA) and analyzed for the expression levels of *eva1*, *cd15*, *sox2* and *cd49f*.

Statistical analysis

Survival data were analyzed for significance by Kaplan-Meier methods using GraphPad Prism version 4 software (*p* values were calculated by the log-rank test). In vitro studies were analyzed by two-tailed Student's *t*-test, with significant difference defined as $p<0.05$.

Results

Eva1 was identified as a novel GIC marker

We first examined the expression of *eva1* in mGICs, NSCL61 and OPCL61, and hGICs, E2, E3 and E6 that were prepared from human GBM tissues (8,10), using RT-PCR. As shown in Figure 1A, *eva1* expression was higher in GICs than in their control cells, mNSC, mOPC and normal hNSC. We confirmed the increased Eva1 expression in human and mouse GICs by western blotting (Fig. 1*B*) and qRT-PCR (Fig. 1*B*, S1*A* and S1*B*). Immunocytochemical analysis revealed that over 90% of cultured human and mouse GICs were positive for Eva1 (Fig. 1*C* and S2*C*, respectively). These Eva1-positive cells existed in human GBM and were co-immunolabeled for a well-known NSC marker Sox2 (>80%, Fig. 1*D*), a GIC marker CD15 (Fig. 1*E*) and CD49f (Fig. 1*F*) (22-24). Flow cytometric analysis showed that 2.1% of the freshly prepared GBM cells were Eva1+ and that about 70% and 50% of Eva1+ cells were also positive for CD15 and CD49f, respectively (Fig. 1*G* and *H*). We further found that Eva1 was undetectable in the adult mouse brain (P100), although it was restrictedly expressed in developing mouse neuroepithelial cells (at E18 and P1) that included multipotent NSCs (25-27) (Fig. S2*D*). Taken together, these results indicated that Eva1 is a potential GIC marker.

Eva1 was prominently expressed in GBM, but not in other gliomas, such as anaplastic oligodendroglioma (AO, WHO grade III), anaplastic oligoastrocytoma (AOA, WHO grade III), or oligodendroglioma (OLI, WHO grade II) (Fig. 2*A* and *B*). The cBioPortal Data (http://www.cbioportal.org/index.do?cancer_study_list=&cancer_study_id=all&data_priority=0&case_ids=&gene_set_choice=user-defined-list&gene_list=&clinical_param_selection=null&tab_index=tab_visualize) (22,21)

suggested that the prognosis of GBM patients with elevated *eva1* mRNA levels (black dashed line, Z-score>2) was worse than the other (gray solid line); median survival and median disease free of the patients (dashed black line) with elevated eva1 was 10.41 and 2.89 months (M), whereas those of the other (solid gray line) was 12.98 and 7 M, respectively (Fig. 2*C*). The Cancer Genome Atlas (TCGA) analysis (http://cancergenome.nih.gov) further revealed that expression of *eva1* significantly increased in GBM compared with the lower grade glioma (LGG), whereas that of CD15, Sox2 or CD49f did not (Fig. 2*D*). These results suggested that Eva1 is a new prognostic marker for GBM.

Eva1 was involved in the GIC proliferation and tumorigenesis

We analyzed the function of Eva1 in GICs using *eva1* and its specific shRNA (*sh1* and *sh2*) expression vectors (Fig. S3). Overexpression of *eva1* increased the expression of stemness genes, *sox2*, *cd15* and *cd49f*, and the self-renewal activity in GICs, whereas its knockdown blocked these activation (Fig. 3*A*-*C*, S4*A* and S4*B*). hGICs formed malignant tumor with hypercellularity and mitosis when injected into the brains of immunodeficient mice, whereas the *eva1sh*-expressing cells did not and the mice injected with the *eva1sh*-expressing GICs survived over 3 months (Fig. 3*C*, data not shown). In addition, enforced expression of *eva1* increased self-renewal activity in hGICs (Fig. S4*B*) and enhanced tumorigenicity of two primary human gliomasphere lines established from AO (Fig. 3*D* and *E*) and diffuse astrocytoma (DA, WHO grade II, Fig. 3*F* and *G*), both of which were Eva1-negative. These Eva1-overexpressing AO and DA cells killed mice more quickly (30 and 55 days, respectively, n=6) than their parental cells (over 60 and 90 days, respectively, to form tumors, n=6) (Fig. 3*E* and *G*, respectively) when inoculated into the immunodeficient

mice intracranially. Together, these results clearly indicated that Eva1 is involved in the GIC proliferation and tumorigenesis.

Eva1 increased the expression of stemness-related genes and the side population through the NF-κB activation in GICs

In order to identify the molecular mechanism that regulated by Eva1, we compared the gene expression profile of NSCL61 with that of *eva1sh*-expressing NSCL61. We found that 1,208 genes were upregulated while 650 were downregulated in *eva1sh*-expressing NSCL61 (Fig. S5*A*). We noted a significant down-regulation in the expression of stemness-related genes, including *aldehyde dehydrogenase 1a3 (aldh1a3)*, *Hairy/enhancer-of-split related with YRPW motif protein 1 (hey1), notch 4*, *jagged 1 (jag1)*, *cytokine receptor 4 (cxcr4)*, *pr domain containing 16 (prdm16)* and *syndecan 1 (sdc1)*. The expression of the ATP-Binding Cassette (ABC) transporter G2 (*abcg2)* also decreased in the *eva1sh*-expressing NSCL61 (Log2 ratio: -0.6). Using RT-PCR, we confirmed the decreased expression level of stemness-related genes, *aldh1a3*, *hey1*, *prdm16, notch4* and *abcg2* in *eva1sh*–expressing NSCL61 (Fig. S5*B*). These results suggested that Eva1 widely regulates the stemness-related gene expression in GICs. Indeed, overexpression of Eva1 increased the SP in hGICs (E3: 21% -> 41%, E6: 22% -> 43%), whereas that of *eva1sh* abolished the population (E3: 22% -> 0.3% (sh1) and 1.9% (sh2), E6: 24% -> 0.3% (sh1) and 1.2% (sh2)) (Fig. 4*A* and *B*). Eva1 level also affected Nestin expression in hGICs and its knockdown significantly increased the differentiation marker-positive cells (Fig. 4*C*-*F*). Apparently, these data indicated that Eva1 is involved in the stemness maintenance in GICs.

Network Analysis software in MetaCore^{TM} (GeneGO) revealed that the

knockdown of Eva1 in NSCL61 influenced the expression of a number of oncogenic transcription networks, including p53, Hypoxia-inducing factor 1α (HIF1α), c-Myc, Nuclear factor-kappa B (NF-κB), and STAT3 (Fig. S5*C*). Of these, we focused on NF-κB because the Eukaryotic Linear Motif resource for Functional Sites in Proteins (ELM) database (http://elm.eu.org/) indicated that the cytoplasmic region of Eva1 contains a consensus binding site for TRAF2, a key regulator in the NF-κB signaling pathway (28), and the Champion ChiP Transcription Factor Search Portal based on the SABiosciences' proprietary database (http://www.sabiosciences.com/chipqpcrsearch.php) indicated that Eva1-downstream stemness-related genes, *aldh1a3*, *hey1*, *notch4*, *jag1*, *cxcr4* and *sdc1*, contain the putative NF-κB binding sites.

To evaluate whether Eva1 activates the NF-κB signaling pathway, we inserted four copies of a NF-κB response element into a reporter vector that contained a minimal SV40 promoter upstream of the firefly luciferase gene. We also constructed two other reporter vectors that contain four copies of a response element for AP1 and SP1 transcription factors, both of which were affected the most in *eva1sh*-expressing NSCL61. We transfected these vectors into NSCL61 and found the increased luciferase activity when transfected with the NF-κB-reporter vector (white columns in Fig. S6*A*). We also detected the NF-κB-dependent luciferase activity in hGICs (white columns in Fig. 5*A*). Using *eva1sh*- and *eva1*-overexpressing hGICs and NSCL61, we found that NF-κB-dependent luciferase activity correlated with Eva1 levels (Fig. 5*A* and *B* and Fig. S6*A* and *B*). To further verify the role of NF-κB signaling in GICs, we used two NF-κB inhibitors, caffeic acid phenethyl ester (CAPE) and pterostilbene (29,30). These inhibitors dramatically blocked the proliferation of both hGIC and NSCL61 in a dose-dependent manner (Fig. 5*C* and *D* and Fig. S6*C*). In addition,

CAPE also inhibited the proliferation of Eva1-overexpressing DA cells, while it partially repressed the proliferation of parental cells (Fig. 5*E*). Taken together, these findings revealed that the Eva1 plays a role in the stemness maintenance of GICs and their proliferation through the activation of NF-κB signaling pathway.

The non-canonical NF-κB signaling pathway is essential for GIC proliferation and tumorigenesis

The receptor-mediated activation of NF-κB has been shown to induce the expression of many genes that regulate inflammation, cell proliferation, immune responses, and tumorigenesis through either canonical or non-canonical signaling pathways (31,32). RelA/p50NF-κB1 and RelB/p52NF-κB2 complexes have been identified as key components in the canonical and non-canonical NF-κB signaling pathways, respectively, while the receptor-binding protein TRAF2 was shown to regulate both pathways (28,31,32). We addressed which of these pathways was crucial for GICs. Using *rela*- and *relb*-shRNA expression vectors (*relash* and *relbsh*, respectively) (Fig. S7*A*), we found that the depletion of RelB, but not RelA, inhibited the NF-κB–dependent luciferase activity in hGICs and NSCL61 (Fig. 6*A* and Fig. S7*B*, respectively). The knockdown of RelB also blocked the proliferation of E3, NSCL61 and Eva1-overexpressing DA cells and the self-renewal activity of hGICs (Fig. 6*C*, S7*C* and S4C, respectively, data not shown for Eva1-expressing DA cells). In addition, RelB knockdown completely abolished tumorigenesis of NSCL61 *in vivo* (Fig. S7*D*). We further found the increased levels of RelB, NIK, a key non-canonical NF-κB-inducing kinase (28,31,32), and the mature form (p52) of NF-κB2 (immature form: p100) in primary human GBM tissues (Fig. 6*D*). Furthermore, prognosis of GBM patients with elevated *relB* mRNA levels (red line) was worse than the others (blue

line) (Fig. S8*A*, Z-score>2) and the expression of *relB* significantly increased in GBM compared with in LGG (Fig. S8*B*). Together, these data indicated that RelB is essential for GIC proliferation and tumorigenesis.

Eva1 activated the non-canonical NF-κB signaling pathway through NIK stabilization and NF-κB2 maturation in GICs

To confirm whether Eva1 activates the RelB-dependent non-canonical NF-κB pathway, we used the Eva1-overexpressing DA cells. As shown in Figure 6*E*, Eva1-overexpression significantly increased the level of RelB, NIK and the mature form of NF-κB2 (p52) in DA cells. A previous study reported that NIK was destabilized by a complex with TRAF2, TRAF3 and the cellular inhibitor of apoptosis (cIAP), while TRAF2 and cIAP were degraded by the proteasome in the receptor-mediated NF-κB–activation pathway (33). Together with that Eva1 cytoplasmic tail contains a putative TRAF2 binding site, these suggest that Eva1 sequesters the TRAF2 and cIAP-containing complex and induces its degradation, thereby resulting in the accumulation of NIK in GICs. To examine this possibility, we cultured Eva1-overexpressing DA cells in the presence or absence of a proteasome inhibitor (PI) and found that both TRAF2 and cIAP were co-immunoprecipitated with Eva1 only in the presence of PI (Fig. 6*F*). These results indicated that Eva1 directly activates the non-canonical NF-κB signaling pathway through the TRAF2/cIAP degradation-dependent NIK accumulation in GICs (Fig. 6*G*).

Discussion

Eva1 was originally identified as an immunoglobulin superfamily member expressed on the developing thymus epithelial cells and was shown to be involved in the T cell development in the early embryo (12,13). Because Eva1 knockout mice did not show any detectable phenotypes (15, Ohtsu et al, unpublished observation), Eva1 is dispensable for the embryonic development, including hematogenesis and neurogenesis. Using human and mouse GIC models, we demonstrated here that Eva1 induces GIC proliferation and tumorigenesis through the activation of RelB-dependent non-canonical NF-κB signaling pathway. Since Eva1 was shown to act as a homophilic binding protein, GICs may be influenced by the Eva1-expressing surround cells, and vice versa. Indeed, we found that RORγT (Th17-determinating transcription factor)-expressing T-helper 17 cell (Th17), which behave as either pro-tumorigenic or anti-tumorigenic cells depending on their internal and external factors, was positive for Eva1 and associated with Eva1+/RORγT– cells in human GBM tissues (34-40, Fig. S9). Our findings suggest that Th17 cells act as tumor-supporting cells through Eva1-dependent intercellular association with GICs. In turn, it is feasible that GICs induce Th17 differentiation by activating the RelB pathway, which is necessary for the induction of RORγT, and supplying TGFβ1 and IL6 (40,41). Thus, it is essential to further investigate the reciprocity between GICs and their surrounding cells, including Th17 cells, through Eva1-trans-homophilic binding in the GBM niche.

The DNA microarray results obtained in the present study revealed that Eva1 induces the expression of a number of stemness-related genes, including Notch-related factors and ABCG2, and activates stemness-related signaling pathways, such as STAT3, in GICs. In fact, we confirmed that Eva1 overexpression increased the SP

and Nestin-positive cells in hGICs, whereas Eva1 knockdown not only decreased the population but also induced neural differentiation in hGICs. Since it is well-known that Notch and STAT3 signaling pathways play essential roles for the stemness maintenance (42-45), Eva1 may also exploit these signaling pathways as well as the NF-κB one for the GICs maintenance.

The molecular mechanism underlying the expression of *eva1* in GICs has yet to be elucidated. The combination of ionomycin and phorbol 12-myristate 13-acetate (PMA) was shown to induce the expression of *eva1* in $CD4^+$ T cells (46). However, AP1, a well-known transcription factor activated by PMA (47), was not activated in NSCL61 (as shown in the present study) and there is no consensus binding sites for the PMA/ionomycin-target transcription factors (NFAT and NF-κB) in the *eva1* 5' genomic region. The Champion ChiP Transcription Factor Search Portal revealed that the *eva1* 5' genomic region contains the binding sites for cancer- and stemness-related transcription factors, such as c-Myc and STAT3, therefore whether these candidate transcription factors actually regulate the expression of *eva1* in GICs should be determined in future studies.

Aberrant canonical and non-canonical NF-κB signalings were previously reported in various types of solid tumors including GBM (48-50). NF-κB activation has been further shown to make GICs be resistant to irradiation through the acquirement of mesenchymal phenotypes (50). We found that E3 is the proneural type of GIC, which strongly express *olig2*, *dll3* and *ascl1*, whereas E6 is the mesenchymal type one, which prominently express *serpine1*, *chi3l1* (also known as *ykl40*), *vegfc* and *runx1*, although non-canonical NF-κB signaling was activated in both GICs. Together, these findings suggested that non-canonical NF-κB signaling could not induce mesenchymal phenotypes in GICs (10, data not shown). Nonetheless, since the

ablation of non-canonical NF-κB signaling could block GIC proliferation and their tumorigenesis, the specific inhibitor for the pathway can be a promising new therapeutic drug for GBM.

Acknowledgments

We thank Martin Raff for his helpful suggestions and critical reading of the manuscript, and Satoshi Kondou for performing the DNA microarray and pathway analyses.

Authors' contribution

Conception and design: T. Kondo

Development of methodology: T. Kondo

Acquisition of data: N. Ohtsu, Y, Nakatani, D. Yamashita, T. Kondo

Analysis and interpretation of data: N. Ohtsu, Y, Nakatani, T. Kondo

Writing and review: T. Kondo

Material support: D. Yamashita, S. Ohue, T. Ohnishi,

Study supervision: T. Kondo

Grant Support

This work was supported, in part, by the Japan Advanced Molecular Imaging Program (J-AMP) and a research program of the Project for Development of Innovative Research on Cancer Therapeutics (P-DIRECT), Ministry of Education, Culture, Sports, Science and Technology of Japan, to T.K.

References

1. Singh SK, Clarke ID, Terasaki M, Bonn VE, Hawkins C, Squire J, et al. Identification of a cancer stem cell in human brain tumors. Cancer Res 2003;63:5821-8.
2. Singh SK, Clarke ID, Hide T, Dirks PB. Cancer stem cells in nervous system tumors. Oncogene 2004;23:7267-73.
3. Kondo T. Brain cancer stem-like cells. Eur J Cancer 2006;42:1237-42.
4. Vescovi AL, Galli R, Reynolds BA. Brain tumour stem cells. Nat Rev Cancer 2006;6:425-36.
5. Lathia JD, Mack SC, Mulkearns-Hubert EE, Valentim CL, Rich JN. Cancer stem cells in glioblastoma. Genes Dev 2015:29;1203-17.
6. Alvarez-Buylla A, Lois C. Neuronal stem cells in the brain of adult vertebrates. Stem Cells 1995;13:263-72.
7. Frisén J, Johansson CB, Lothian C, Lendahl U. Central nervous system stem cells in the embryo and adult. Cell Mol Life Sci 1998;54:935-45.
8. Hide T, Takezaki T, Nakatani Y, Nakamura H, Kuratsu J, Kondo T. Sox11 prevents tumorigenesis of glioma-initiating cells by inducing neuronal differentiation. Cancer Res 2009;69:7953-9.
9. Hide T, Takezaki T, Nakatani Y, Nakamura H, Kuratsu J, Kondo T. Combination of a Ptgs2 inhibitor and an EGFR signaling inhibitor prevents tumorigenesis of oligodendrocyte lineage derived glioma-initiating cells. Stem Cells 2011;29:590-9.
10. Yamashita D, Kondo T, Ohue S, Takahashi H, Ishikawa M, Matoba R, et al. miR340 Suppresses the Stem-like Cell Function of Glioma-Initiating Cells by Targeting Tissue Plasminogen Activator. Cancer Res 2015;75:1123-33.
11. Kaneko S, Nakatani Y, Takezaki T, Hide T, Yamashita D, Ohtsu N, et al. Ceacam1L modulates STAT3 signaling to control the proliferation of glioblastoma-initiating cells.

Cancer Res In press.

12. Guttinger M, Sutti F, Panigada M, Porcellini S, Merati B, Mariani M, et al. Epithelial V-like antigen (EVA), a novel member of the immunoglobulin superfamily, expressed in embryonic epithelia with a potential role as homotypic adhesion molecule in thymus histogenesis. J Cell Biol 1998;141:1061-71.
13. Iacovelli S, Iosue I, Di Cesare S, Guttinger M. Lymphoid EVA1 expression is required for DN1-DN3 thymocytes transition. PLoS One 2009;4:e7586.
14. DeMonte L, Porcellini S, Tafi E, Sheridan J, Gordon J, Depreter M, et al. EVA regulates thymic stromal organisation and early thymocyte development. Biochem Biophys Res Commun 2007;356:334-40.
15. Wright E, Rahgozar K, Hallworth N, Lanker S, Carrithers MD. Epithelial V-like antigen mediates efficacy of anti-alpha integrin treatment in a mouse model of multiple sclerosis. PLoS One 2013;8:e70954.
16. Kondo T, Raff M. Chromatin remodeling and histone modification in the conversion of oligodendrocyte precursors to neural stem cells. Genes Dev 2004;18:2963-72.
17. DiDonato JA, Mercurio F, Karin M. NF-κB and the link between inflammation and cancer. Immunol Rev 2012;246:379-400.
18. Thomas M, Klibanov AM. Enhancing polyethylenimine's delivery of plasmid DNA into mammalian cells. Proc Natl Acad Sci USA 2002;99:14640-5.
19. Takanaga H, Tsuchida-Straeten N, Nishide K, Watanabe A, Aburatani H, Kondo T. Gli2 is a novel regulator of sox2 expression in telencephalic neuroepithelial cells. Stem Cells 2009;27:165-74.
20. Cerami E, Gao J, Dogrusoz U, Gross BE, Sumer SO, Aksoy BA, et al. The cBio cancer genomics portal: an open platform for exploring multidimensional cancer genomics data. Cancer Discov 2012;2:401-4

21. Gao J, Aksoy BA, Dogrusoz U, Dresdner G, Gross B, Sumer SO, et al. Integrative analysis of complex cancer genomics and clinical profiles using the cBioPortal. Sci Signal. 2013;6:pl1.
22. Gangemi RM, Griffero F, Marubbi D, Perera M, Capra MC, Malatesta P, et al. SOX2 silencing in glioblastoma tumor-initiating cells causes stop of proliferation and loss of tumorigenicity. Stem Cells. 2009;27:40-8.
23. Son MJ, Woolard K, Nam DH, Lee J, Fine HA. SSEA-1 is an enrichment marker for tumor-initiating cells in human glioblastoma. Cell Stem Cell 2009;4:440-52.
24. Lathia JD, Gallagher J, Heddleston JM, Wang J, Eyler CE, Macswords J, et al. Integrin alpha 6 regulates glioblastoma stem cells. Cell Stem Cell. 2010;6:421-32.
25. Temple S. Division and differentiation of isolated CNS blast cells in microculture. Nature 1989;340:471-3.
26. Lendahl U, Zimmerman LB, McKay RD. CNS stem cells express a new class of intermediate filament protein. Cell 1990;60:585-95.
27. Doetshe F, Caillé I, Lim DA, García-Verdugo JM, Alvarez-Buylla A. Subventricular zone astrocytes are neural stem cells in the adult mammalian brain. Cell 1999;97:703-16.
28. Shih VF, Tsui R, Caldwell A, Hoffmann A. A single NF-κB system for both canonical and non-canonical signaling. Cell Res 2011;21:86-102.
29. Natarajan K, Singh S, Burke TR. Jr, Grunberger D, Aggarwal BB. Caffeic acid phenethyl ester is a potent and specific inhibitor of activation of nuclear transcription factor NF-kappa B. Proc Natl Acad Sci USA 1996;93:9090-5.
30. Priego S, Feddi F, Ferrer P, Mena S, Benlloch M, Ortega A, et al. Natural polyphenols facilitate elimination of HT-29 colorectal cancer xenografts by chemoradiotherapy: a Bcl-2- and superoxide dismutase 2-dependent mechanism. Mol Cancer Ther 2008;7:3330-42.
31. Baud V, Karin M. Is NF-kappaB a good target for cancer therapy? Hopes and pitfalls. Nat

Rev Drug Discov 2009;8:33-40.

32. Gyrd-Hansen M, Meier P. IAPs: from caspase inhibitors to modulators of NF-kappaB, inflammation and cancer. Nat Rev Cancer 2010;10:561-74.
33. Vallabhapurapu S, Matsuzawa A, Zhang W, Tseng PH, Keats JJ, Wang H, et al. Nonredundant and complementary functions of TRAF2 and TRAF3 in a ubiquitination cascade that activates NIK-dependent alternative NF-kappaB signaling. Nat Immunol 2008;9:1364-70.
34. Su X, Ye J, Hsueh EC, Zhang Y, Hoft DF, Peng G. Tumor microenvironments direct the recruitment and expansion of human Th17 cells. J Immunol 2010;184:1630-41.
35. Kryczek I, Wu K, Zhao E, Wei S, Vatan L, Szeliga W, et al. IL-17+ regulatory T cells in the microenvironments of chronic inflammation and cancer. J Immunol 2011;186:4388-95.
36. Wilke CM, Kryczek I, Wei S, Zhao E, Wu K, Wang G, et al. Th17 cells in cancer: help or hindrance? Carcinogenesis 2011;32:643-9.
37. Qi W, Huang X, Wang J. Correlation between Th17 cells and tumor microenvironment. Cell Immunol 2013;285:18-22.
38. Xiang T, Long H, He L, Han X, Lin K, Liang Z, et al. Interleukin-17 produced by tumor microenvironment promotes self-renewal of CD133+ cancer stem-like cells in ovarian cancer. Oncogene 2013;34:165-76.
39. Song X, Gao H, Lin Y, Yao Y, Zhu S, Wang J, et al. Alterations in the microbiota drive interleukin-17C production from intestinal epithelial cells to promote tumorigenesis. Immunity 2014;40:140-52.
40. Powolny-Budnicka I, Riemann M, Tänzer S, Schmid RM, Hehlgans T, Weih F. RelA and RelB transcription factors in distinct thymocyte populations control lymphotoxin-dependent interleukin-17 production in γδ T cells. Immunity 2011;34:364-74.
41. Li MO, Wan YY, Flavell RA. T cell-produced transforming growth factor-beta1

controls T cell tolerance and regulates Th1- and Th17-cell differentiation. Immunity 2007;26:579-91.

42. Morrison SJ. Neuronal potential and lineage determination by neural stem cells. Curr Opin Cell Biol 2001;13:666-72.
43. Gaiano N, Fishell G. The role of notch in promoting glial and neural stem cell fates. Annu Rev Neurosci 2002;25:471-90.
44. Fan X, Matsui W, Khaki L, Stearns D, Chun J, Li YM, et al. Notch pathway inhibition depletes stem-like cells and blocks engraftment in embryonal brain tumors. Cancer Res 2006;66:7445-52.
45. Voskas D, Ling LS, Woodgett JR. Signals controlling un-differentiated states in embryonic stem and cancer cells: role of the phosphatidylinositol 3' kinase pathway. J Cell Physiol 2014;229:1312-22.
46. Wojcik E, Carrithers LM, Carrithers MD. Characterization of epithelial V-like antigen in human choroid plexus epithelial cells: potential role in CNS immune surveillance. Neurosci Lett 2011;495:115-20.
47. Macián F, García-Cózar F, Im SH, Horton HF, Byrne MC, Rao A. Transcriptional mechanisms underlying lymphocyte tolerance. Cell 2012;109:719-31.
48. Sun SC. Non-canonical NF-κB signaling pathway. Cell Res 2011;21:71-85.
49. Mauro C, Leow SC, Anso E, Rocha S, Thotakura AK, Tornatore L, et al. NF-kB control energy homeostasis and metabolic adaptation by upregulating mitochondrial respiration. Nat Cell Biol 2011;13:1272-9.
50. Bhat KP, Balasubramaniyan V, Vaillant B, Ezhilarasan R, Hummelink K, Hollingsworth F, et al. Mesenchymal differentiation mediated by NF-κB promotes radiation resistance in glioblastoma. Cancer Cell 2013;24:331-46.

Figure Legends

Figure 1. Eva1 is predominantly expressed in GICs

A, *Eva1* expression in mouse control cells ($p53^{-/-}$ mNSCs and mOPCs), mouse GICs (NSCL61 and OPCL61), hNSCs and hGICs (E3 and E6) was examined by RT-PCR. The expression of *gapdh* was used as an internal control. **B,** A western blotting analysis of Eva1 expression in the cells examined in (**A**). **C,** Representative data of hGICs immunostained for Eva1 (green) and Nestin (red). **D-F,** Primary human GBM specimens, immunostained for Eva1 (green) and Sox2 (red) (**D**), CD15 (red) (**E**) or CD49f (red) (**F**). **G,** Representative data from an expression analysis of Eva1 and either CD15 (left panel) or CD49f (right panel) in one of three human GBMs by flow cytometry. **H,** Ratio of the Eva1/CD15- and Eva1/CD49f-double positive cells in human GBM tissues (n=3). Error bar indicates ±SD. Nuclei were counterstained with DAPI (blue). All experiments were repeated at least three times with similar results. Scale bar: 50 μm, 20 μm (insets).

Figure 2. Eva1 is a novel prognostic marker for malignant glioma

A, The expression of *eva1* in GBM, anaplastic oligodendroglioma (AO), anaplastic oligoastrocytoma (AOA), oligodendroglioma (OLI), hGICs, and control brain tissue (CB) was examined by RT-PCR (40 cycles). The expression of *gapdh* was used as an internal control. **B,** A western blotting analysis of Eva1 expression in glioma examined in (**A**). **C,** Clinical data from the cBioPortal database indicated that increased *eva1* mRNA (black dashed line, Z-score>2) has correlated with a poorer prognosis, survival (left panel) and disease free (right panel), in GBM. **D,** Expression data (27 microarray data) from TCGA database indicated that *eva1* expression significantly increased in GBM, compared with LGG, whereas expression of *cd15*,

sox2 or *cd49f* did not. Error bar indicates ±SD. t test was used for statistical significance. **** $p<0.0001$.

Figure 3. Eva1 is involved in GIC proliferation and tumorigenesis

A, Increased expression of *sox2*, *cd15* and *cd49f*, in *eva1*-overexpressing GICs. **B,** Decreased expression of *sox2*, *cd15* and *cd49f*, in *eva1sh1* and *sh2*-expressing GICs. **C,** Decreased proliferation of *eva1sh*-expressing hGICs, E3 and E6. **D,** Representative photographs of the brains transplanted with either *controlsh* (contsh)-, *eva1sh1*- or *sh2*-expressing E3. Lower panels show the high magnification images. White dashed circle indicates tumor. Similar results were reproduced in six brains for each experiment. **E,** H&E staining of human AO tissue (left panel) and of a tumor formed by *eva1*-expressing AO cells (right panel). **F,** Survival curves for mice injected with AO cells (black dotted line) or *eva1*-expressing AO cells (red solid line). n=6. **G,** H&E staining of human DA tissue (left panel) and of a tumor formed by *eva1*-expressing DA cells (right panel). **H,** Survival curves for mice injected with DA cells (black dotted line) and *eva1*-expressing DA cells (red solid line). n=6. Data are presented as the mean of three independent experiments. Error bar indicates ±SD. t test was used for statistical significance. * $p<0.05$, ** $p<0.01$ and **** $p<0.0001$ significantly different from cells expressing control vectors. Scale bar: 100 μm.

Figure 4. Eva1 levels affected SP and neural marker expression in hGICs

A, Increased SP in *eva1*-overexpressing E3 and E6. **B,** Decreased SP in *eva1sh1*- and *sh2*-overexpressing E3 and E6. Flow cytometry experiments were repeated at least three times with similar results. **C-F,** Ratio of the neural stem/differentiation marker-positive E3 (**C, E**) and E6 (**D, F**). White columns show control cells. Black and gray

columns show *eva1*-(**C, D**), *eva1sh1*- and *sh2*-(**E, F**) overexpressing cells. Data are presented as the mean of three independent experiments. Error bar indicates ±SD. t test was used for statistical significance. * $p<0.05$, ** $p<0.01$, *** $p<0.001$ and **** $p<0.0001$ significantly different from control.

Figure 5. Eva1 regulates the hGIC proliferation through the NF-κB signaling pathway

A, The overexpression of *eva1* increased NF-κB–dependent luciferase activity in E3 and E6. **B,** The overexpression of *eva1sh1* and *sh2* decreased NF-κB-dependent luciferase activity in E3 and E6. **C, D,** NF-κB inhibitors, CAPE (**C**) and Pterostilbene (**D**), inhibited the proliferation of E3 (filled circles) and E6 (filled triangles). Open circles and triangles show the viability of E3 and E6 in the presence of DMSO alone (cont). **E,** CAPE inhibited the proliferation of *eva1*-overexpressing DA cells, and partially prevented that of the parental DA cells. Data are presented as the mean of three independent experiments. Error bar indicates ±SD. t test was used for statistical significance. * $p<0.05$ and ** $p<0.01$ significantly different from control.

Figure 6. Eva1 regulates hGIC proliferation through the RelB/NF-κB2 pathway

A, The overexpression of *relbsh* decreased NF-κB-dependent luciferase activity in E3 and E6. **B, C,** The enforced expression of *relbsh* blocked the proliferation of E3 (**B**) and *eva1*-overexpressing DA cells (**C**). **D,** The expression of NIK, NF-κB2, RelA, and RelB in the control brain (CB) and GBM tissue was analyzed by Western blotting. **E,** The overexpression of *eva1* stabilized NIK, increased RelB, and induced the processing of immature NF-κB2 (p100) into the mature form (p52) in DA cells. **F,** Endogenous TRAF2 and cIAP co-immunoprecipitated with exogenous Eva1 in the

presence of a proteasome inhibitor (PI) in DA cells. **G,** A model of Eva1-dependent activation of the non-canonical NF-κB signaling pathway. The experiments were repeated at least three times with similar results. Error bar indicates ±SD. t test was used for statistical significance. * $p<0.05$, ** $p<0.01$, *** $p<0.001$ and **** $p<0.0001$ significantly different from cells expressing control shRNA (*contsh*).

Ohtsu et al, Figure 1

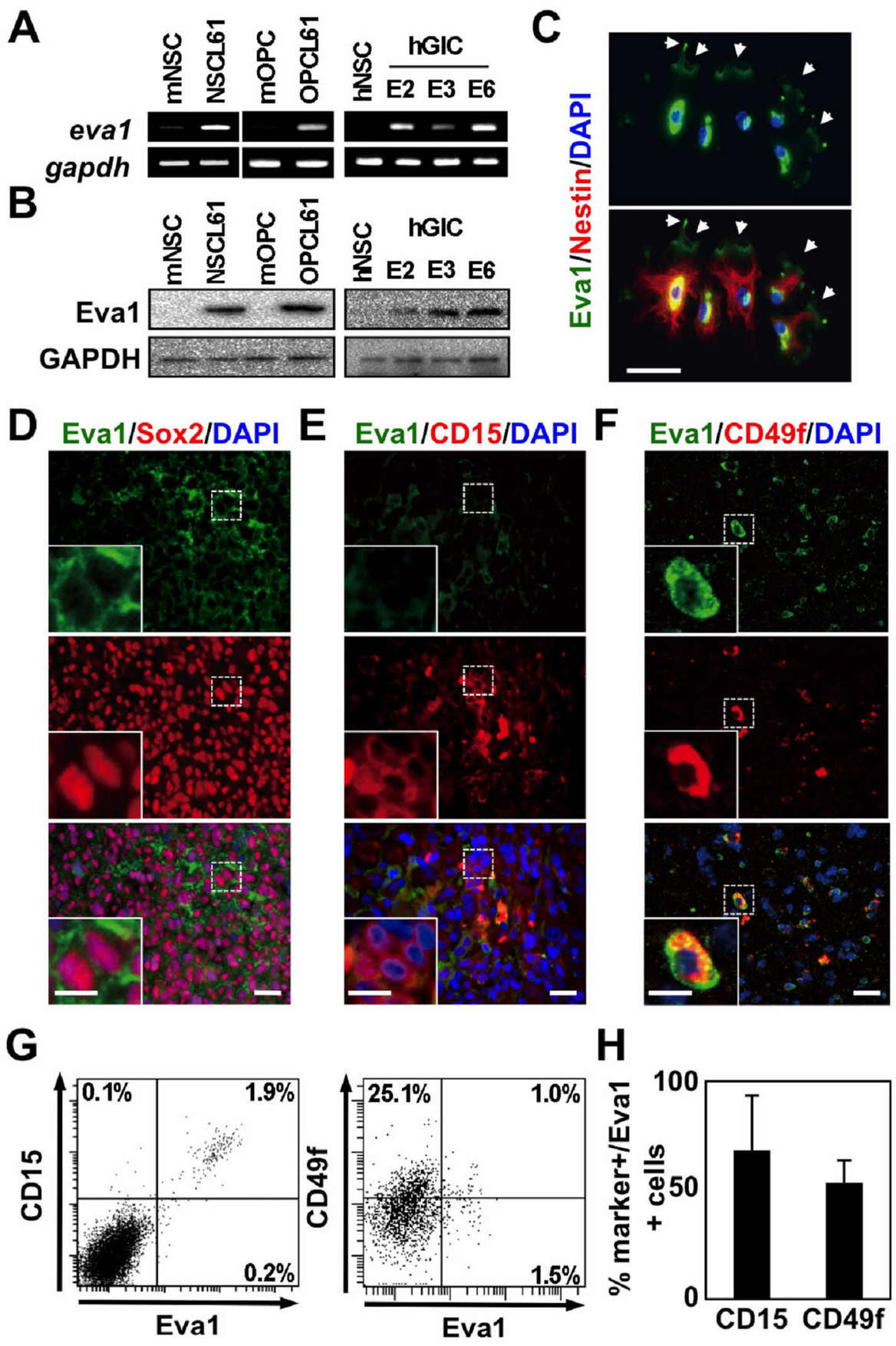

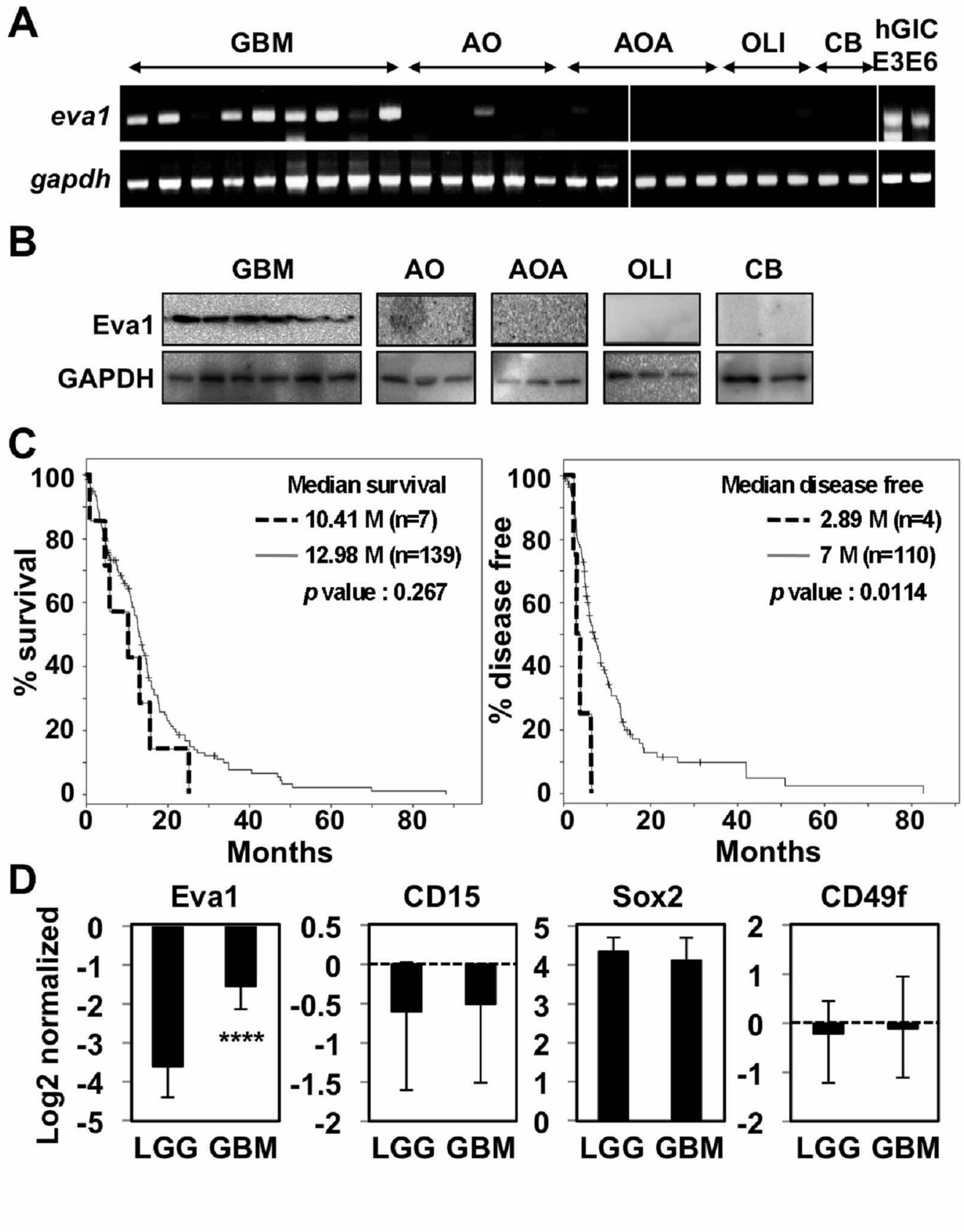
A
GBM
AO
AOA
OLI
CB
hGIC E3E6
eva1
gapdh
B
GBM
AO
AOA
OLI
CB
Eva1
GAPDH
C
Median survival
10.41 M (n=7)
12.98 M (n=139)
p value : 0.267
% survival
Months
Median disease free
2.89 M (n=4)
7 M (n=110)
p value : 0.0114
% disease free
Months
D
Eva1
CD15
Sox2
CD49f
Log2 normalized
****
LGG GBM

Ohtsu et al, Figure 3

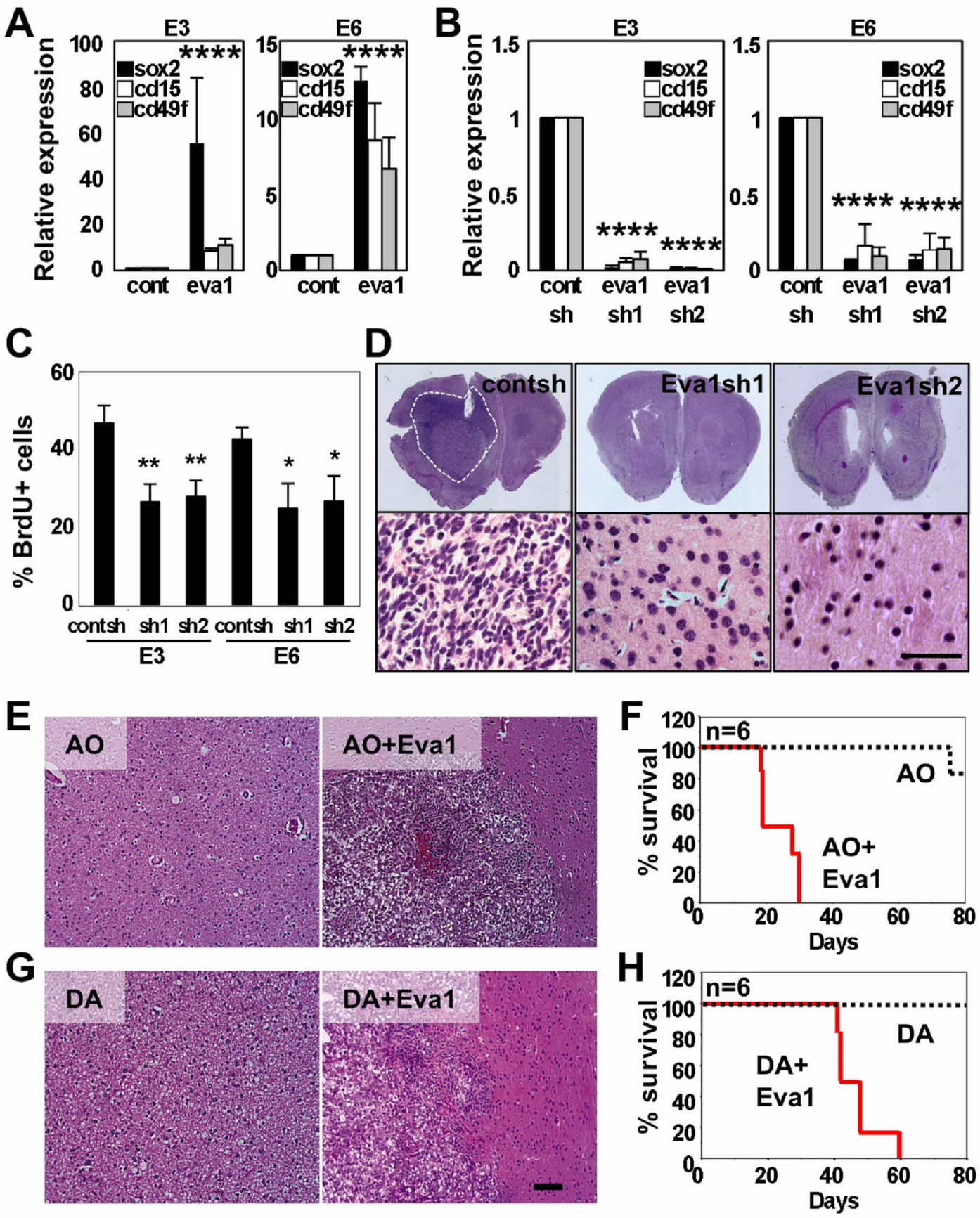

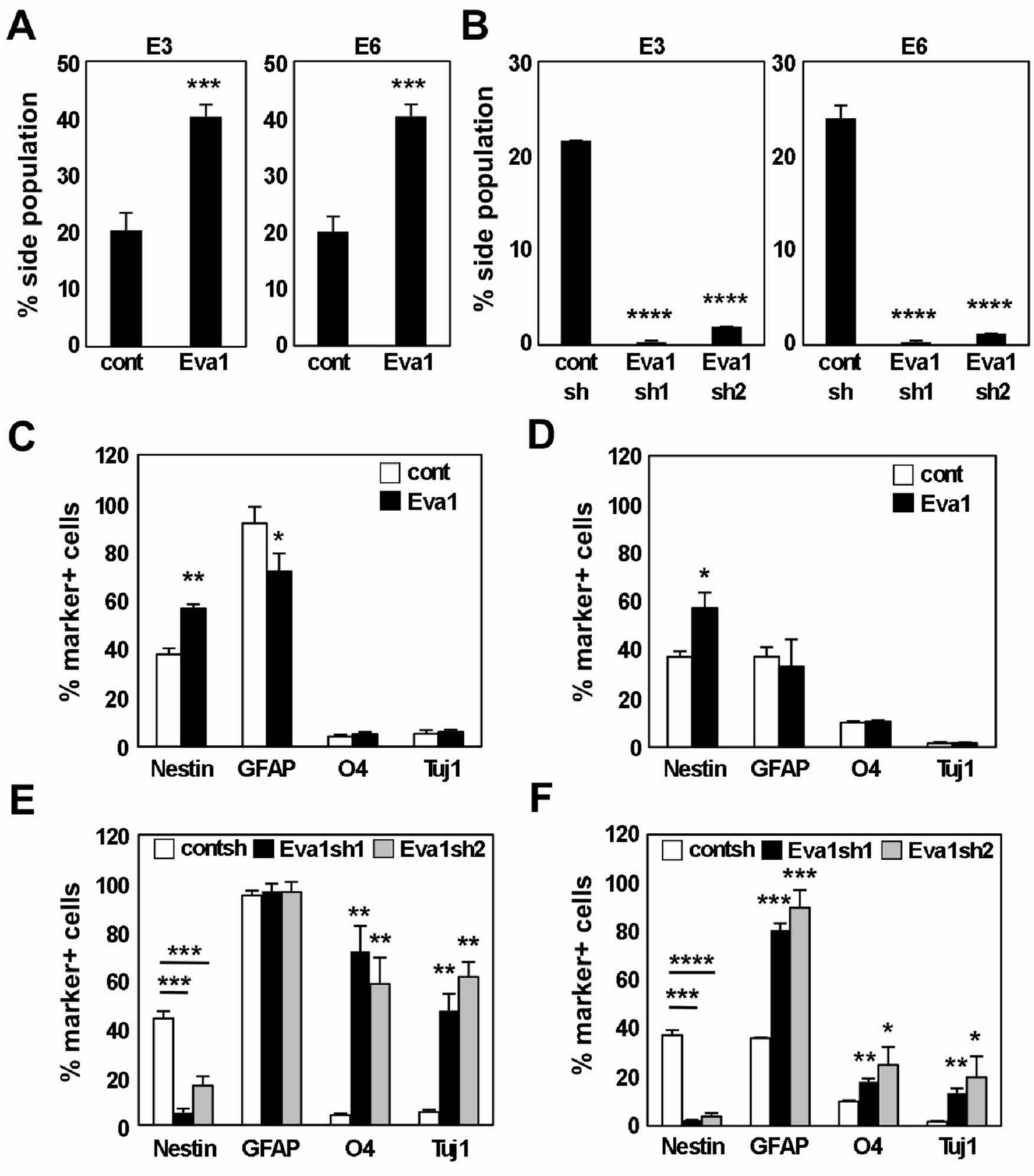
A
E3
E6
% side population
50
40
30
20
10
0
***
cont
Eva1
B
E3
E6
% side population
30
20
10
0
****
cont
Eva1
sh
Eva1
sh1
Eva1
sh2
C
% marker+ cells
120
100
80
60
40
20
0
cont
Eva1
**
*
Nestin
GFAP
O4
Tuj1
D
% marker+ cells
*
E
contsh
Eva1sh1
Eva1sh2
***
**
F
****

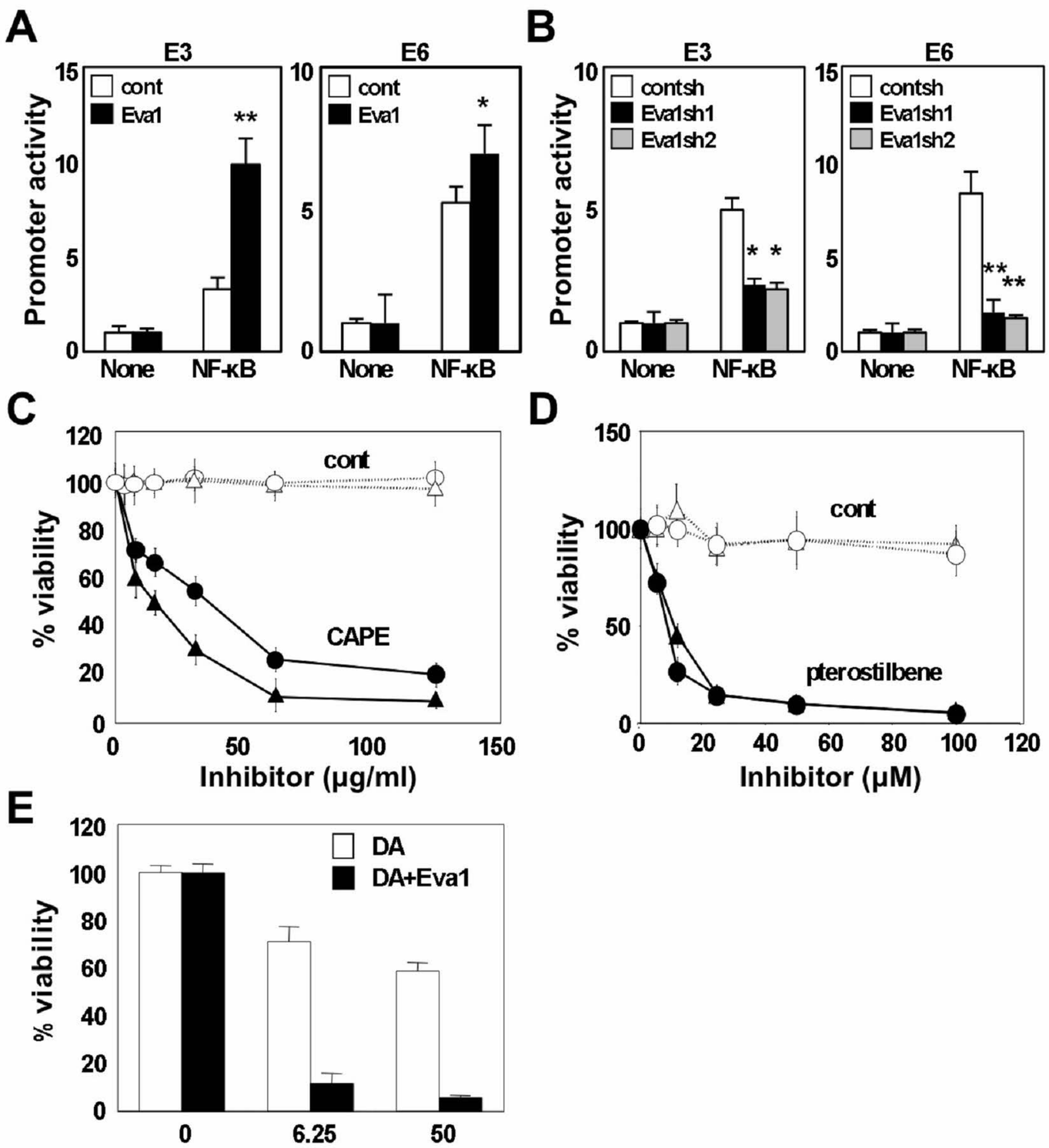
A
E3
E6
cont
Eva1
Promoter activity
None
NF-κB
B
contsh
Eva1sh1
Eva1sh2
C
cont
CAPE
% viability
Inhibitor (μg/ml)
D
pterostilbene
Inhibitor (μM)
E
DA
DA+Eva1
CAPE (μg/ml)

Ohtsu et al, Figure 6